Underwater Ultrasonic Multipath Diffraction Model for Short Range Communication and Sensing Applications

Fabian John, Marco Cimdins, and Horst Hellbrück

***Abstract*—In acoustic underwater communication and sonar applications, obstacles inside and outside the line-of-sight (LOS) affect signal propagation. Both reflection and diffraction occur in underwater communication and measurement systems due to these obstacles. To the best of our knowledge, the influence of diffraction and reflection is neither described nor modeled for finite pulses yet. We propose and develop a multipath propagation model for spectral diffraction components and phase information of the received signal based on knife-edge diffraction together with reflections, transmission effects, and backscatter. This paper designs a short range underwater ultrasonic experimental system composed of an ultrasonic transceiver with wideband pulses and advanced spectral signal processing. We evaluate our proposed model with measurements made in a water tank with an obstacle moved between the transmitter and receiver. When the model includes all major propagation components and effects, it achieves an accuracy for localization of 97% of the results in the range of twice the obstacle diameter in our test setup.**

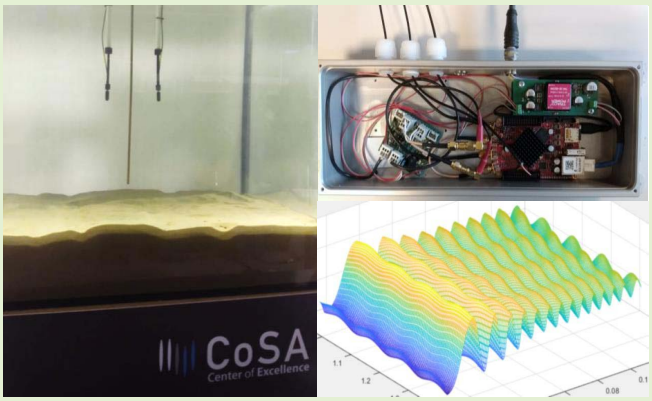

***Index Terms*—Multipath, processing of acoustic wave sensor data, propagation model, spectral diffraction model, ultrasonic sensors, underwater, wideband pulse.**

I. Introduction

MULTIPATH propagation, including scattering, reflection, and diffraction from objects, and backscattering from sediment layers have been investigated in ultrasonic wave propagation [1]–[3]. All these effects are essential for underwater communication as well as measurement systems. Doppler effects, which often occur in the surface reflection in underwater communications [1], [2], [4], are not yet considered in this work because these effects have no influence in short propagation distances in open water with static transducer positions. Ultrasonic acoustics is part of a funded research project at the Center of Excellence CoSA at the Technische Hochschule Lübeck, where we develop a sensor system for sediment exploration.

For the design of an acoustic sensor, a suitable simulation model is missing. Finite element simulations such as COMSOL are too complex and CPU intensive. Additionally, they do not help to interpret and processing the measurements. Therefore, we propose a propagation model for supporting the design of underwater ultrasonic systems and the interpretation of measurement data. Our model calculates obstacle geometries' effects on a pulse-echo ultrasonic system's received signal for a specific frequency band.

State-of-the-art pulse-echo object localization systems with time-of-flight measurements of reflections and backscatter discard spectral and phase information of the received signal [5], [6]. We will show in this paper that spectral and phase information help in the future to systematically design communication systems and other applications such as underwater sediment exploration.

In acoustic underwater communication, multipath propagation is a challenge, as waves propagate with different velocities and frequencies depending on the attenuation along each

Manuscript received June 28, 2021; accepted August 31, 2021. Date of publication September 3, 2021; date of current version October 18, 2021. This work was supported by the Federal Ministry of Economic Affairs and Energy of the Federal Republic of Germany through the Project EXTENSE and Project Management Agency: Jülich (PTJ) under Grant 03SX467B. The associate editor coordinating the review of this article and approving it for publication was Dr. Abhishek K. Jha. *(Corresponding author: Fabian John.)*

Fabian John and Marco Cimdins are with the Center of Excellence CoSA, Technische Hochschule Lübeck, 23562 Lübeck, Germany (e-mail: fabian.john@th-luebeck.de; marco.cimdins@th-luebeck.de).

Horst Hellbrück is with the Center of Excellence CoSA, Technische Hochschule Lübeck, 23562 Lübeck, Germany, and also with the Institute of Telematics, University of Lübeck, 23562 Lübeck, Germany (e-mail: horst.hellbrück@th-luebeck.de).

Digital Object Identifier 10.1109/JSEN.2021.3110005

path [1], [7], [8]. Multipath propagation leads to constructive and destructive interferences, which are distributed over the frequency band used and influence the acoustic communication channel [1], [4], [9]. Caused by the low propagation speed of the waves ($\approx 1500 m/s$), the impact of the Doppler-shift is higher compared to free-space radio frequency propagation and challenges underwater communication. For the fixed transducer setup in this work and measurements in open water without bottom and surface reflections, modeling of the Doppler effect was omitted.

Our proposed model enables us to determine the ultrasonic propagation and evaluate different obstacles such as cables on the received signal. Inspired by the device-free localization model in [10], we present an extended analytical model for underwater ultrasonic wave propagation. The original radio propagation model provides a multipath fading channel's complex value based on knife-edge diffraction of obstacles.

This paper transfers the knife-edge diffraction model developed for radio frequency-based localization to underwater ultrasonic applications. Also, we extend the model with reflectors [11], transmission through the obstacle in between the line-of-sight (LOS), wideband pulses, and time finite signals with phase accurate superposition.

Our proposed model calculates the spectral behavior on the received signal of a pulse-echo ultrasonic system in the presence of an obstacle in the XY plane for a static situation. The definition of multipath components in our model to build complex propagation channels is shown in Section II. The combination of diffraction and reflection explains measurement results from other papers [12]–[14]. To the best of our knowledge, such a combination has not been presented before, and our results show the importance of diffraction effects in multipath propagation channels.

Our model combines knife-edge diffraction and reflections to simulate the ultrasonic underwater multipath propagation and the effect of different obstacles in the proximity of the transmission. Furthermore, we summarize related work regarding ultrasonic sensing and diffraction effects in non-underwater applications as medical and geophysical imaging and underwater detection and localization applications.

The application of ultrasonic transceivers is common in medical applications. Image reconstruction algorithms exploit ultrasonic diffraction to show the object of interest surrounded by an array of ultrasonic transducers. The Born or Rytov approximations, which are valid for weakly scattering objects, are used to linearize the reconstruction equations [15]–[17]. Placing receiver arrays behind the object is not applicable for underwater applications, such as localizing buried objects within the sediment or surrounding an underwater communication multipath channel. In underwater applications, strong diffraction effects on objects have been observed. Simultaneously, strong backscatter effects from sediments and Doppler-shifts can be assumed, which precludes using the Born or Rytov approximation to linearize the system equations [1]–[4].

Devaney transferred the medical imaging to geophysical imaging methods, considering a modified arrangement of transmitters and receivers in a borehole, and contributed the geophysical diffraction tomography with the limitation to weakly inhomogeneous formations [18]. However, transducer arrangements within the borehole do not apply to underwater applications because the sensors are moved at a distance from the seafloor without touching it. In non-destructive testing, ultrasonic time-of-flight diffraction is an established method to detect and visualize cracks inside materials [19], [20]. This method requires that the transmitter and receiver rotate around or are behind the object, which is also not applicable for underwater applications. However, the work demonstrates the importance of diffraction effects for ultrasonic propagation.

In the following, we will provide information about related work regarding underwater applications of ultrasonic systems and diffraction effects. Localization of buried objects with time-of-flight ultrasonic systems, such as subbottom profilers, is based on the target object's backscatter. Beamforming, i.e., variations of beam angles or transducer arrays, are employed to increase resolution and minimize these systems' signal-to-noise ratio [21]–[23]. Disturbances caused by backscatter or reverberation of the surrounding environment (e.g., sediment ripples) limit such systems' performance [14], [21], [23]. For visualization, the systems calculate the received signal's envelope, which discards spectral and phase information.

Capus *et al.* present a spectral approach for underwater object detection and characterization. Their method is based on Lamb wave propagation around a cylindrical object [13], [14]. The cable curvature, tank wall returns, sediment surface, and ambient noise explain this method's limitations to cable tracking applications [13].

To the best of our knowledge, diffraction effects are listed as sources of disturbances in other underwater applications [14], [21], [23], but are not yet investigated and modeled yet. We develop a multipath propagation model for spectral diffraction components and phase information and evaluate it with measurements with a transmitter and receiver and an obstacle. Our model and the performed measurements show the strength of the diffraction effects in a short-range setup in free water without bottom, surface, and tank wall reflections.

The contributions of the paper are: we develop a multipath propagation model that accounts for spectral diffraction components and phase information of the received signal, together with reflections, transmission effects, and backscatter. Furthermore, we propose adapting the parameters of our analytical model to apply to our measurement setup. We evaluate our proposed model with short range measurements made in a saltwater tank with an obstacle moved outside the transmitter and receiver's LOS.

The rest of the paper is structured as follows: We develop the propagation model in Section II. Section III describes the measurement setup and the model parameters adapted to the real scenario. Section IV presents the results and discussion. Finally, in Section V, we conclude the paper and provide an outlook for future work.

II. Ultrasonic Multipath Pulse-Echo Model

In this section, we derive an ultrasonic propagation model for a static transmitter and receiver setup. Our model includes three types of propagation paths diffraction, transmission

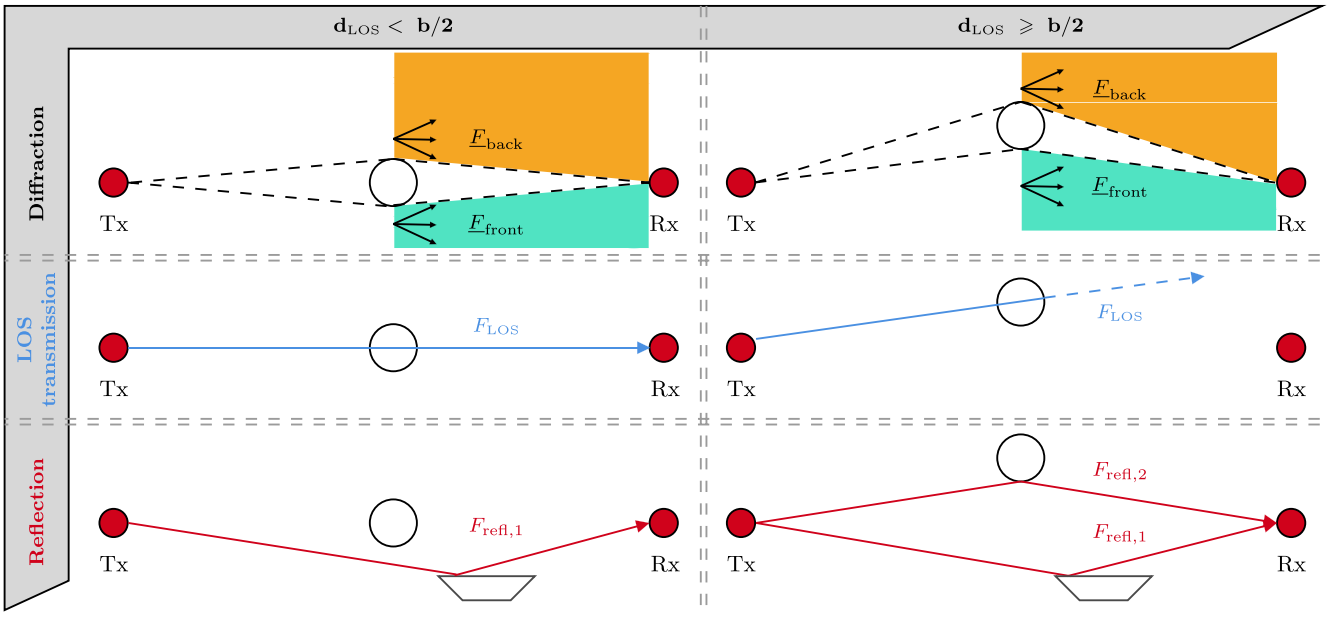

Fig. 1. Signals of the multipath ultrasonic pulse echo model; black signals: knife-edge diffraction; blue signals: transmitted through the obstacle; red signals: reflected signals.

through an obstacle, and reflections for multipath propagation. According to the multipath propagation scenario, the multipath components are instantiated in any number in our model. For detailed information about the models' implementation, we refer to the repository.[1] The propagation of an ultrasonic wave in the presence of an obstacle is divided into two cases when the object appears (a) inside and (b) outside the line-of-sight (LOS). We consider the physical effects of diffraction, transmission through the obstacle, and reflection in our model (see Fig. 1). Knife-edge diffraction occurs at the edges of the obstacle, both inside and outside the LOS, and is described in Section II-A. We model the signal that crosses through the obstacle as LOS transmission component in Section II-B, for the obstacle in between the LOS. Reflections caused by the obstacle and other static reflectors are shown in Fig. 1 and included in the model in Section II-C. The total received signal is the superposition in the time-domain of the diffraction, LOS transmission, and reflection components. We present the signal components' cutting and the phase's correction to model signals of pulse-echo systems with finite behavior in the time domain. This leads to an accurate superposition of the phase in Section II-D.

Fig. 2 illustrates the model in a block diagram. The black-colored blocks in the left line in Fig. 2 model the diffraction effects as shown in the top line in Fig. 1. The blue blocks in the middle in Fig. 2 model the transmission through the obstacle shown in the middle in Fig. 1 and the red blocks at the right in Fig. 2 model the reflected signal components as shown in Fig. 1.

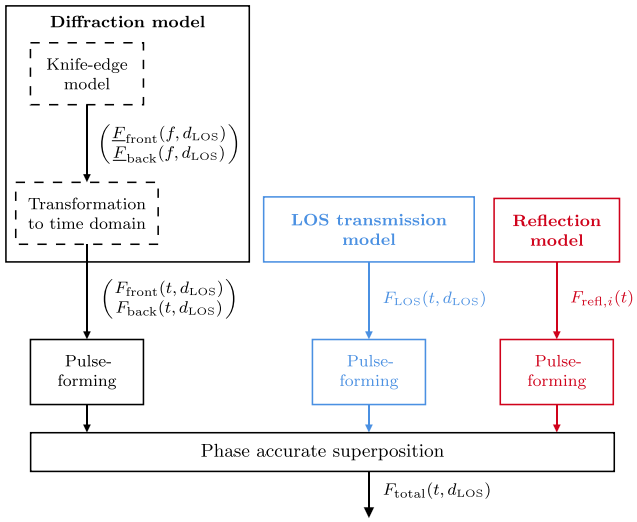

Fig. 2. Block diagram of the ultrasonic pulse-echo model in the time-domain; black blocks: diffraction components; blue blocks: transmission through the obstacle in LOS; red blocks: reflection components.

A. Diffraction Model

In this section, we derive the diffraction model for ultrasonic pulse-echo systems. The diffraction model describes how an obstacle alters the signal transmitted by Tx and measured by Rx. The knife-edge model has been initially derived for a radio frequency-based system [11] in 2017. The knife-edge model describes the influence on the magnitude and phase of an obstacle, such as a person, on the transmitted radio waves. For further information on the diffraction model for a device-free localization system, we refer to [10].

Fig. 3 shows the topology and the parameters. The model requires the position of the transmitter Tx, and receiver Rx, and the diameter b, and position $\mathbf{x}$ of the cylindrical obstacle. Depending on those positions within the XY plane, we calculate the distance d_{LOS} from the direct line between the transmitter Tx and the receiver Rx towards the position of

[1] https://git.mylab.th-luebeck.de/fabian.john/us_multipath_model.git

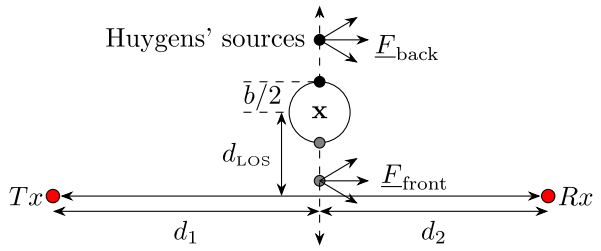

Fig. 3. Topology of the knife-edge diffraction model ©2019 IEEE, adapted from [25]. The original model was introduced in [11].

the obstacle **x**. d_1 is the vector projection from Tx to **x**, and d_2 is the vector projection from **x** towards Rx. Equation (1) calculates the Fresnel-Kirchoff parameter based on those values [24].

$$v = d_{\text{LOS}}\sqrt{\frac{2\cdot(d_1+d_2)}{\lambda d_1 d_2}} \tag{1}$$

where λ is the wavelength of the transmitted signal. The wavelength λ is calculated as $\lambda = c/f$, where c is the speed of the wave within the medium and f is the frequency.

The knife-edge diffraction model determines the effect of an obstacle on the propagation. An assumption is that the propagating wave cannot pass the obstacle. The propagation continues due to emerging Huygens' sources at the edges of the obstacle (see Fig. 3).

The complex Fresnel integral $\underline{F}(v)$ is defined as the ratio between the electric field E measured at the receiver and the free-space electric field E_0 [24]. For our underwater ultrasonic system, we adapt the complex Fresnel integral $\underline{F}(v)$ as the ratio between the pressure intensity P measured at the receiver and the free-space pressure intensity P_0.

$$\underline{F}(v) = \frac{P}{P_0} = \frac{1+j}{2}\left[\left(\frac{1}{2}-C(v)\right) - j\left(\frac{1}{2}-S(v)\right)\right] \tag{2}$$

$C(v)$ is the Fresnel cosine and the $S(v)$ the Fresnel sine, respectively. Both values are dependent on the Fresnel-Kirchhoff parameter v that we calculate with (1) based on the geometry of the setup.

Fig. 3 shows that the obstacle has a cylindrical shape. Therefore, we calculate the Fresnel integral $\underline{F}_{\text{front}}(-v_{\text{front}})$ that describes the pressure intensity from the front of the obstacle towards $-\infty$ and the Fresnel integral $\underline{F}_{\text{back}}(v_{\text{back}})$ that calculates the pressure intensity from the back of the obstacle towards ∞. v_{back} is calculated with (1) and $d_{\text{LOS,back}} = d_{\text{LOS}} + b/2$, v_{front} with $d_{\text{LOS,front}} = d_{\text{LOS}} - b/2$, respectively.

The components $\underline{F}_{\text{front}}(v_{\text{front}})$ and $\underline{F}_{\text{back}}(v_{\text{back}})$ of the propagation model characterize the diffraction effects, caused by an obstacle, to a signal for a given frequency. In [10], the complex Fresnel integrals were calculated for the center frequency of an ultra-wideband pulse to model the total attenuation of the signal for a device-free localization application. We describe the enhancement and application of the free-space diffraction model for underwater (pulse-echo) multipath propagation in the rest of this section. For our underwater propagation model, we derive a wideband pulse from these $\underline{F}_{\text{front}}(v_{\text{front}})$ and $\underline{F}_{\text{back}}(v_{\text{back}})$ components, taking the finite behavior of the pulse in time-domain into account. Therefore, we transfer the complex components back into the time-based representation. We also calculate the signal components for all included frequencies of the wideband pulse, so that the attenuation can be evaluated spectrally if needed. For the following steps, it is important to keep in mind that the components $\underline{F}(v) = \underline{F}(d_{\text{LOS}}, f)$ characterize the attenuation of a received signal with an obstacle at d_{LOS} related to a received signal without obstacle, at a dedicated frequency f.

Considering real pulse-echo systems, we estimate a pulse in a given frequency range $f = [f_{\text{low}}; f_{\text{high}}]$. In the time-domain, the attenuation $F(t, d_{\text{LOS}})$ of this frequency range is the superposition of the component in this range:

$$F(t, d_{\text{LOS}}) = \int_{f_{\text{low}}}^{f_{\text{high}}} \left|\underline{F}(f, d_{\text{LOS}})\right| \cdot \sin\Bigg(2\pi f t + \arctan \times \left(\frac{\text{Im}(\underline{F}(f, d_{\text{LOS}}))}{\text{Re}(\underline{F}(f, d_{\text{LOS}}))}\right)\Bigg)\, df \tag{3}$$

The components $F_{\text{front}}(t, d_{\text{LOS}})$ and $F_{\text{back}}(t, d_{\text{LOS}})$ are calculated with (2) and (3). Further processing of these components, as pulse-forming and the phase accurate superposition with other multipath components, account for the time finite properties of the pulse and different arrival times for each path. As shown in Fig. 2, pulse-forming and phase accurate superposition is performed for all multipath components and is described in Section II-D.

B. LOS Transmission Model

To model the obstacle's transmission characteristics, we divide the model into two cases: (a) the obstacle is inside and (b) the obstacle is outside of the LOS. For the obstacle inside the LOS, the received pressure intensity depends on the obstacle section that the LOS crosses. The crossed section $d_{\text{obstacle}}(d_{\text{LOS}})$ of a circular shaped obstacle in the position d_{LOS} is calculated with

$$d_{\text{obstacle}}(d_{\text{LOS}}) = 2\cdot\cos\left(\frac{d_{\text{LOS}}}{b/2}\pi\right). \tag{4}$$

For the obstacle located at $d_{\text{LOS}} = 0$, we define the transmission factor $F_{\text{LOS}}(t, 0) = F_{0,\text{LOS}}$. Then the transmission factor for the obstacle inside the LOS depends on $d_{\text{obstacle}}(d_{\text{LOS}})$ and $F_{0,\text{LOS}}$ in (5).

For the obstacle outside the LOS, the signal paths that are obstructed by the object will not reach the receiver (refer Fig. 1, right part in LOS transmission). We calculate the transmission factor for all obstacle positions with

$$F_{\text{LOS}}(d_{\text{LOS}}) = \begin{cases} F_{0,\text{LOS}}\cdot\cos\left(\pi\dfrac{d_{\text{LOS}}}{b/2}\right), & |d_{\text{LOS}}| \le \dfrac{b}{2} \\ 0, & |d_{\text{LOS}}| > \dfrac{b}{2}. \end{cases} \tag{5}$$

Corresponding to the diffraction model, the transmission factor $F_{\text{LOS}}(d_{\text{LOS}})$ is the received signal relative to the measured pressure intensity without the obstacle. To account for all the frequencies within the bandwidth of the wideband pulse,

we calculate the signal in the time-domain with

$$F_{\mathrm{LOS}}(t, d_{\mathrm{LOS}}) = \int_{f_{\mathrm{low}}}^{f_{\mathrm{high}}} F_{\mathrm{LOS}}(d_{\mathrm{LOS}}) \cdot \sin(2\pi f t)\, df. \tag{6}$$

Modeling the pulse-echo system's finite behavior in the time-domain is described in Section II-D. In the next section, we describe the modeling of reflected signal components.

C. Reflection Model

Objects, seafloor, and surface reflect ultrasonic waves in underwater applications. Each reflection path adds a multipath signal component with a path-dependent attenuation and propagation delay at the receiver [1], [2], [4]. In this section, we present an extended reflection model based on N reflectors. We define a reflector i as an acoustic reflecting object in a static or moving position to the transmitter-receiver pair. A typical static reflector is the mechanical mounting of the transducers, and a typical moving reflector is an obstacle in the proximity of the transmission channel.

Modeling a received pulse from a reflector i follows the approach described in Section II-A. We assume a wideband pulse with a given frequency range $f = [f_{\mathrm{low}}; f_{\mathrm{high}}]$ that is described by the path depended attenuation R_i and phase angle $\phi_{\mathrm{refl}} = \pi$ [rad]. We calculate the reflected pulse component in the time-domain with

$$F_{\mathrm{refl},i}(t) = \int_{f_{\mathrm{low}}}^{f_{\mathrm{high}}} R_i \cdot \sin(2\pi f t + \pi)\, df. \tag{7}$$

The path-dependent propagation delay for each multipath component is considered with a phase accurate superposition. In the following section, we superimpose the effects of diffraction, LOS transmission, reflection, and the finite behavior of the ultrasonic pulse-echo system in the time domain.

D. Pulse Forming and Phase Accurate Superposition

The signal components F_{front}, F_{back}, F_{LOS}, and $F_{\mathrm{refl},i}$ of the previous sections, have an infinite behavior in the time-domain. To adapt these components to a pulse-echo system's finite behavior in the time domain, we cut the signal components to the desired pulse length. We apply a window function with smoothing behavior to avoid artificial high frequencies caused by cutting in the time domain. The Hanning window function $w_{\mathrm{Hann}}(t)$ provides a smoothing behavior [26] and is used in our model to cut the infinite signal components (8). We apply the length T_{pulse} of the desired pulse-echo system as the Hanning window function's length.

$$F^{\sqcap}(t) = w_{\mathrm{Hann}}(t) \cdot F(t) \tag{8}$$

In the following, we account for different propagation paths d_{path} with individual lengths to achieve an accurate phase of the signal components. The delay τ_{path}, when the signal component arrives at the receiver, depends on the length of the propagation path d_{path} and the velocity of the ultrasonic wave c in

$$\tau_{\mathrm{path}} = \frac{d_{\mathrm{path}}}{c}. \tag{9}$$

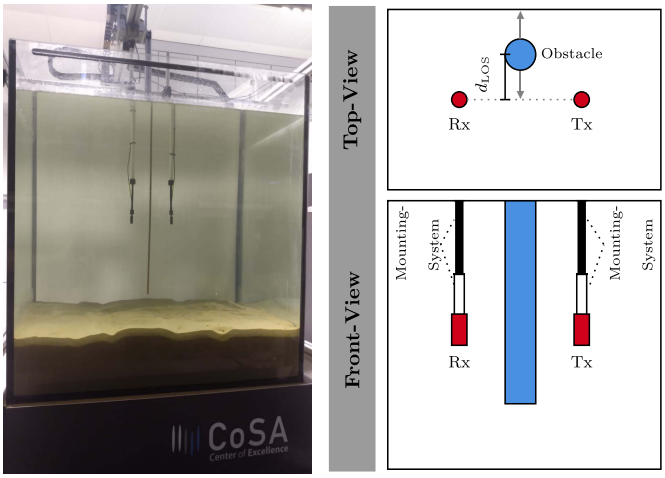

(a) Front view. (b) Schematic top and front view.

Fig. 4. Measurement setup.

Finally, we calculate the attenuation $F_{\mathrm{total}}(t, d_{\mathrm{LOS}})$ by the superposition of the time finite signal components $F^{\sqcap}_{\mathrm{front}}(t, d_{\mathrm{LOS}})$, $F^{\sqcap}_{\mathrm{back}}(t, d_{\mathrm{LOS}})$, $F^{\sqcap}_{\mathrm{LOS}}(t, d_{\mathrm{LOS}})$, and $F^{\sqcap}_{\mathrm{refl},i}(t)$, with respect to the individual time-shift τ_{path} of each multipath component. The modeling of complex multipath propagation is achieved in the model by an arbitrary configurable number of refection components with path individual attenuation and delay. We superpose the signals with accurate phase in (10).

$$\begin{aligned} &F_{\mathrm{total}}(t, d_{\mathrm{LOS}}) \\ &\quad = F^{\sqcap}_{\mathrm{front}}(t - \tau_{\mathrm{front}}, d_{\mathrm{LOS}}) + F^{\sqcap}_{\mathrm{back}}(t - \tau_{\mathrm{back}}, d_{\mathrm{LOS}}) \\ &\qquad + F^{\sqcap}_{\mathrm{LOS}}(t - \tau_{\mathrm{LOS}}, d_{\mathrm{LOS}}) + \sum_{i}^{N} F^{\sqcap}_{\mathrm{refl},i}(t - \tau_{\mathrm{refl},i}) \end{aligned} \tag{10}$$

The output of our ultrasonic multipath pulse-echo model is the attenuation F_{total} in the time-domain, which is related to the idle measurement without an obstacle.

III. Measurements

Our proposed model calculates the propagation of ultrasonic waves in the presence of an obstacle. To evaluate our propagation model and demonstrate the diffraction effects, caused by the obstacle, we perform measurements in a saltwater tank with a size of $60cm \times 80cm \times 50cm$ (length, width, and water height). The dimensions and positioning of the transducers with a distance of $12cm$ were chosen, that the number of multipath components is reduced. Therefore the evaluation of the model is simplified, but the measurements represent only a short communication range for underwater communication application and object localization in free water.

Fig. 4 shows the measurement setup, as well as the schematic top and front view.

The transducer system is located in the middle of the tank. The signal acquisition stopped at $300\mu s$, before reflections from the tank walls, water-air top layer, and water-sediment bottom layer arrived (fastest arrival from water-air top layer with a path length of $\approx 50cm$ at $t = 340\mu s$). Therefore, we do not consider these reflections during the adaption of the propagation model's parameters in Section III-D.

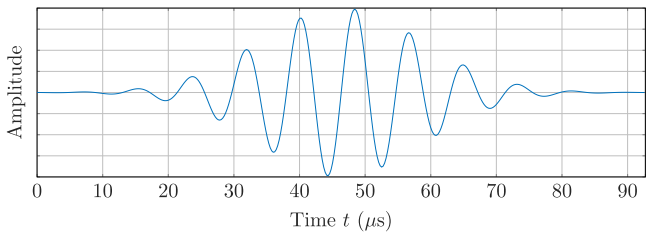

(a) Time-domain.

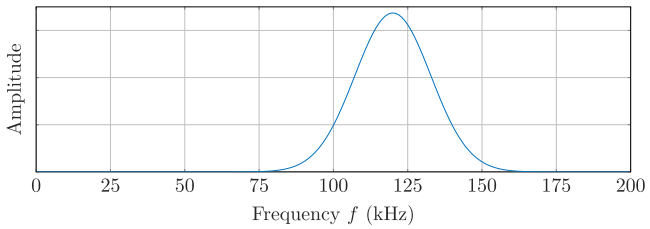

(b) Frequency-domain.

Fig. 5. Transmitted Gaussian-modulated sinusoidal pulse $f_0 = 120\,\text{kHz}$, $b_{3\,\text{dB}} = 30\,\text{kHz}$.

We chose the setup to investigate the different effects on the ultrasonic propagation due to an obstacle. In the future, we will apply this model to cables that are buried within the sediment. This requires the inclusion of other effects, such as refraction, that are out of this paper's scope.

A. Implementation

The transmitter-receiver system is mounted in a fixed position in the tank at the mounting of an automated XY-positioning system. As an obstacle, we employ a cylindrical copper bar with $b = 0.6cm$ diameter that is mounted to the automated XY-positioning system. The copper bar is moved perpendicular to the LOS between transmitter and receiver.

During the measurement, the obstacle is incrementally moved to positions in the interval $d_{\text{LOS}} = [0; 12]cm$ with a step size of $\Delta d_{\text{LOS}} = 0.025cm$. This procedure enables us to evaluate small fluctuations of the magnitude and phase of the received signal.

At each position, the obstacle is stopped and a Gaussian-modulated sinusoidal pulse with center frequency $f_0 = 120kHz$ and bandwidth $b_w = 30kHz$ is sent by the transmitter. Besides, the receiver is triggered to start a measurement (see Fig. 5). After completion of one measurement, the obstacle is moved to the next position. We performed the acquisition of the idle measurement without an obstacle mounted on the positioning system.

B. Equipment

The equipment for performance measurements to evaluate our model is listed in Table I. We employed TC4013 hydrophone transducers from Teledyne Marine to generate and measure ultrasonic waves in the underwater measurement setup. These transducers have a frequency range from $1Hz$ up to $170kHz$ with omnidirectional sensitivities for generating and acquiring signals [27].

TABLE I
EQUIPMENT USED FOR EVALUATION MEASUREMENT

Type	Device	Description
Transducer	Teledyne TC4013	Ultrasonic transmitter and receiver
Amplifier	PCB board with OP-Amps	Self designed printed circuit board for analog signal amplification [12]
Data Acquisition	RedPitaya 125-14	Embedded 2 channel oscilloscope and 2 channel signal generator
Signal Generator		
PC	Windows PC with Intel i7	Control and automation unit
Velocity measurement	CTD60Mc probe (Sea and Sun Technology GmbH)	Measurement of the sound velocity during measurements ($c = 1503\ \text{m/s}$)
Tank	Saltwater filled tank	$60\ \text{cm} \times 80\ \text{cm} \times 50\ \text{cm}$ (length, width, and water height)

We calculate the Gaussian-modulated sinusoidal pulse as a waveform with Matlab on a PC. The calculated waveform is sent via message queuing telemetry transport (MQTT) protocol over a TCP/IP connection to the RedPitaya 125-14, an embedded signal generator. A rising edge on the GPIO pin of the RedPitaya 125-14 starts the analog signal output and triggers the analog signal input digitization. We apply a hydrophone amplifier PCB [12], with an amplification factor of 10 to connect the transducers to the analog input and output of the RedPitaya. For signal acquisition, the amplified analog signal is digitized with a sample rate of $15.6MS/s$ and $14Bit$ resolution by the RedPitaya. The two analog channels are read out via an FPGA, and 16384 values are buffered after triggering. The buffer values are transferred via MQTT to the PC as a binary payload (65 kByte packet per channel). Finally, the received waveforms are stored and processed in Matlab on a PC. The positioning system is also controlled by the Matlab script from the PC over MQTT.

C. Signal Processing

We performed an idle measurement $p_0(t)$ without obstacle in the tank to use it as a reference signal for measurements with the obstacle $p(t, d_{\text{LOS}})$ at the different positions. We filter the raw signal's DC offset and cut the received pulse for both the idle measurement and the measurement with an obstacle. Then, we calculate the single sided discrete fast Fourier transformation for the signals as $p_0(f)$ and $p(f, d_{\text{LOS}})$. Finally, we measure the relative pressure intensity for different spectra with $F_{\text{meas}}(f, d_{\text{LOS}}) = 20 \cdot \log_{10}\left(\frac{p(f,d_{\text{LOS}})}{p_0(f)}\right)$.

D. Adaption of the Model Parameters

In Section II, we presented our multipath pulse-echo model. We derived the components from calculating the attenuation for a single transmitter and receiver system in the presence of an obstacle. Table II presents the parameter settings for adapting our model to the measurement setup within a saltwater tank.

The values for the parameters b, d_1, d_2, d_{LOS}, f_{low}, f_{high}, $d_{\text{refl},1}$, and T_{pulse} depend to the measurement setup of the pulse-echo system in Fig. 4. We measured the velocity of ultrasonic waves c, which is dependent on the salinity and

TABLE II
CHOSEN PARAMETERS TO ADAPT THE MODEL AND MEASUREMENTS

Parameter	Value	Description
b	0.6 cm	Obstacle diameter
$d_1 = d_2$	6.2 cm	LOS distance to transducers
d_{LOS}	$[0; 0.025; ...; 12]$ cm	Perpendicular obstacle distance
f_{low}	90 kHz	Lower frequency bound
f_{high}	150 kHz	Upper frequency bound
c	1503 m/s	Velocity of sound
$F_{0,\text{LOS}}$	1	Transmission factor
$d_{\text{refl},1}$	25 cm	Path length of first reflection
R_1	0.15	Factor of first reflection
T_{pulse}	92.71 μs	Length of transmitted pulse

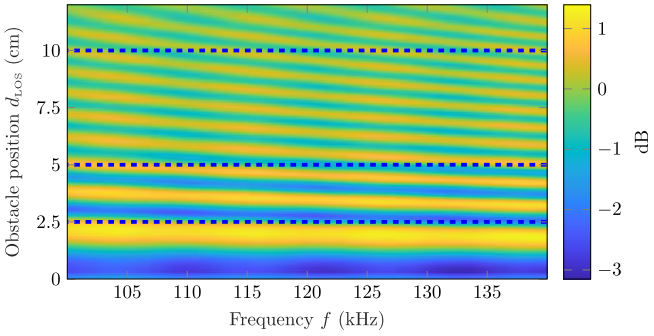

(a) Model.

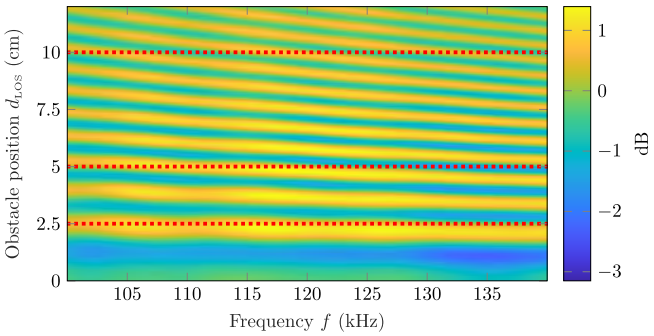

(b) Measurement.

Fig. 6. Spectral results (red and blue lines: exemplary selected signals in Fig. 8).

temperature of the water-filled tank with the CTD60Mc probe from Sea and Sun Technology GmbH. We adapted the parameters $F_{0,\text{LOS}}$ and R_1 empirically during the model's evaluation.

IV. EVALUATION

In Section II, we derived the ultrasonic multipath model for pulse-echo systems and presented in Section III-D the model's adaption to the measurement setup that we use for evaluation. Finally, we process the measured signals to a spectral representation. The model output $F_{\text{total}}(t, d_{\text{LOS}})$ in Section II is in the time-domain. To achieve comparable results, we transform $F_{\text{total}}(t, d_{\text{LOS}})$ to the frequency domain using a single-sided discrete fast Fourier transformation. Fig. 6 shows the calculated results $F_{\text{total}}(f, d_{\text{LOS}})$ from the model in (a) and the measured results in (b) as a ratio in dB.

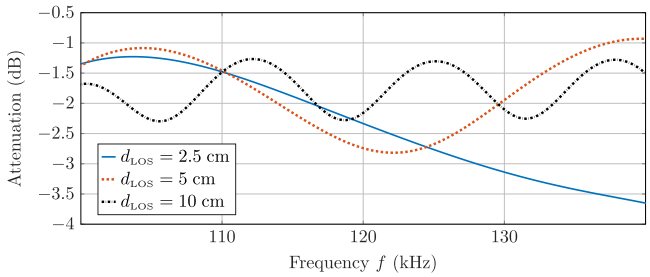

(a) Diffraction.

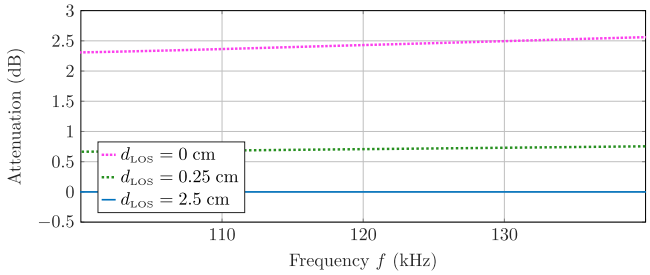

(b) LOS transmission.

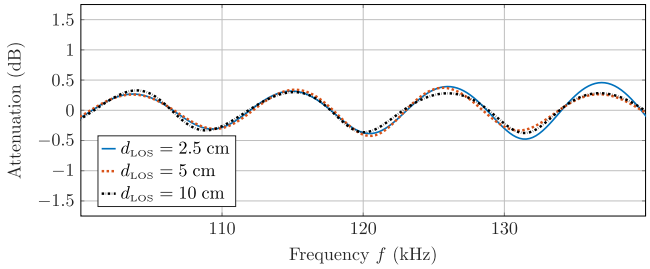

(c) Reflection.

Fig. 7. Spectral characteristics for the modeled components.

For both the model and measurement results, we observe alternating matching color patterns in the horizontal (frequency) and vertical range (obstacle position d_{LOS}). We also observe a clockwise rotation of the vertical alternating characteristic with increasing distance between obstacle d_{LOS} and the transmitter, receiver pair. The spectrum's shape is caused by constructive and destructive interference of the superposition of the diffraction, LOS transmission, and reflection components that we investigated in our model. Fig. 7 shows the characteristic of the spectrum for each component. Diffraction as shown in in Fig. 7(a) results in to the vertical alternating characteristic in Fig. 6, which is rotating clockwise. With an increasing distance of the obstacle d_{LOS}, the alternating minima and maxima of the spectrum change in the amplitude and frequency in Fig. 7(a). The characteristic of the LOS transmission is shown in Fig. 7(b). LOS transmission results in a nearly constant factor depending on the obstacle position. Finally, reflection contributes with an alternating characteristic in the spectrum that is almost independent of the obstacle position d_{LOS} (shown in Fig. 7(c)).

The superposition of the three contributing signal components (diffraction, LOS transmission, and reflection), each shown in Fig. 7, result in qualitatively varying spectra at

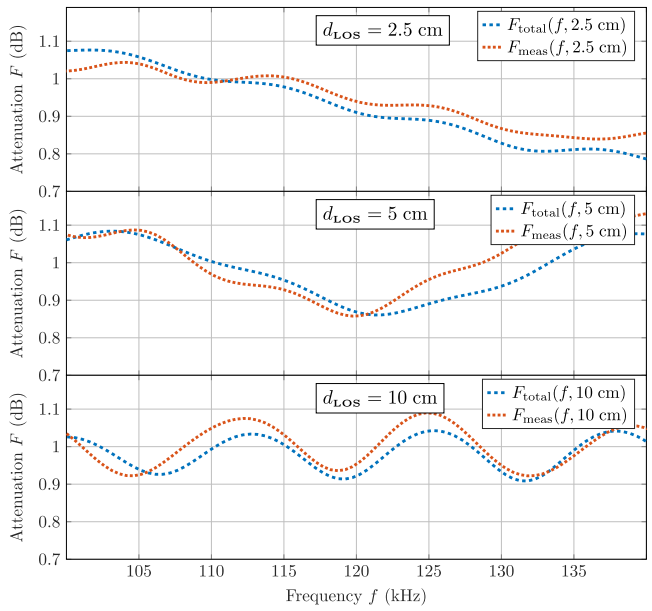

Fig. 8. Modeled and measured signals for different obstacle positions d_{LOS}.

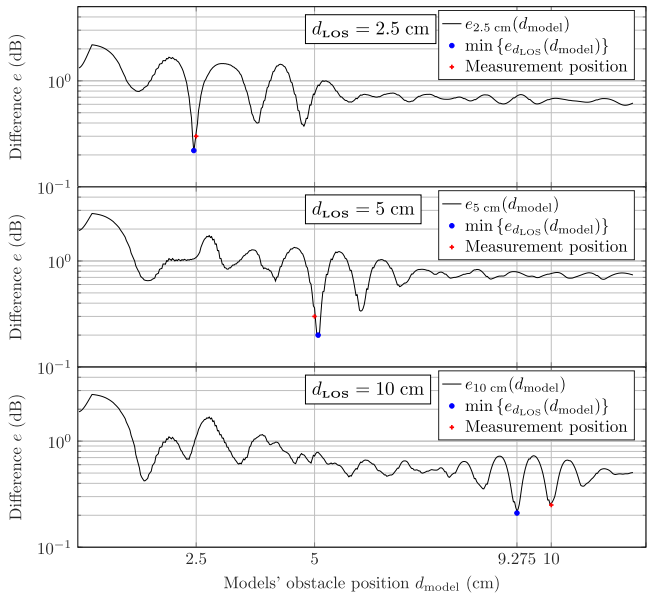

Fig. 9. Mean absolute error for 3 exemplary measured obstacle positions, each compared to all modeled positions.

distinct obstacle positions. We observed qualitatively comparable varying spectra in the measurement and the model and depicted spectra for both at three exemplarily chosen positions in Fig. 8.

In the following, we compare the results of our model with the measurements. For each d_{LOS}, we calculate the difference between the model (dashed blue line) and our measurement (red dotted line) over the frequency range, exemplarily shown in Fig. 8. Inspired by [28], we chose the absolute differences between the two vectors, which is a common metric of spectral fingerprints. The absolute difference $e_{d_{\mathrm{LOS}}}(d_{\mathrm{model}})$ between a measured spectrum and each calculated spectrum is calculated with:

$$e_{d_{\mathrm{LOS}}}(d_{\mathrm{model}}) = \int \left| F_{\mathrm{total}}(f, d_{\mathrm{model}}) - F_{\mathrm{meas}}(f, d_{\mathrm{LOS}}) \right| df \quad (11)$$

Fig. 9 shows the results for $e_{d_{\mathrm{LOS}}}(d_{\mathrm{model}})$ for the three selected obstacle positions $d_{\mathrm{LOS}} = [2.5; 5; 10]cm$. We calculate the position $d_{\mathrm{calculated}}(d_{\mathrm{LOS}})$ from measurements with our model with (12).

$$d_{\mathrm{calculated}}(d_{\mathrm{LOS}}) = \underset{d_{\mathrm{model}}}{\arg\min}\ e_{d_{\mathrm{LOS}}}(d_{\mathrm{model}}). \quad (12)$$

The calculated obstacle position $d_{\mathrm{calculated}}$ is at the absolute minimum of $e_{d_{\mathrm{LOS}}}(d_{\mathrm{model}})$. With $e_{d_{\mathrm{LOS}}}(d_{\mathrm{model}})$, we apply the nearest neighbor algorithm to select the position that minimizes the difference between the result of the model and the measurements.

In Fig. 9 we marked the position, calculated with the nearest neighbor algorithm $d_{\mathrm{calculated}}$ with blue. The measurement position, that was given as ground truth by the automated positioning system during the measurement, is marked in red. For the three positions shown in Fig. 9, the calculated and measured position match with a small deviation for the first and second exemplarily chosen positions $d_{\mathrm{LOS}} = [2.5, 5]cm$.

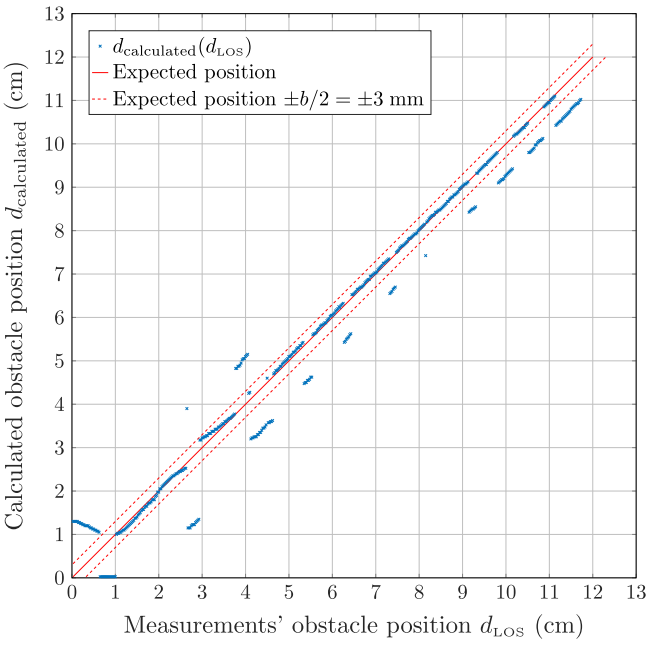

Fig. 10. Calculated positions based on the proposed model.

For the third position at $d_{\mathrm{LOS}} = 10cm$, the calculated position deviate with $0.725cm$, because the function $e_{d_{\mathrm{LOS}}}(d_{\mathrm{model}})$ has an local minimum at the measurement position, and the global minimum located left.

Fig. 10 shows the calculated positions $d_{\mathrm{calculated}}(d_{\mathrm{LOS}})$ for all measurements. The solid red line depicts the reference given by the position setting during the measurement, and the red dashed lines indicate the size of the obstacle diameter b in the plot. At positions with an increased deviation between the calculated position $d_{\mathrm{calculated}}$ and the expected position, the expected position is only a local minimum in the

function $e_{d_{\mathrm{LOS}}}(d_{\mathrm{model}})$, as described for the position $d_{\mathrm{LOS}} = 10cm$ before. This explains the erratic deviations in Fig. 10.

Finally, we calculate the absolute error between the expected position and the model's calculated position as Δd with (13).

$$\Delta d(d_{\mathrm{LOS}}) = |d_{\mathrm{LOS}} - d_{\mathrm{calculated}}(d_{\mathrm{LOS}})| \tag{13}$$

65% of the calculated positions match the position setting from measurement in the range of the obstacle diameter ($|\Delta d(d_{\mathrm{LOS}})| < 0.3cm$). The majority of the values outside those limits are at a distance of $0.7cm - 1.2cm$ from the position setting (see Fig. 10). 97% of the calculated values are less than $\pm 1.2cm$ apart from the expected position, which is twice the size of the obstacle diameter b.

In this section, we evaluated our model by measurements. We applied the nearest neighbor algorithm that results with 97% of the values in a range of twice the size of the obstacle diameter of $1.2cm$. 90% of the calculated results are in the range of $0.975cm$, 80% in the range of $0.750cm$, and 50% in the range of $0.075cm$.

In summary, our model is close to the measurements and performs well.

V. Conclusion and Future Work

In this work, we developed an underwater multipath ultrasonic model that calculates the spectral signal and physical effects of diffraction, transmission, and reflection for a transmitter/receiver pair, and an obstacle for wideband pulses. Diffraction, transmission, and reflection result in constructive and destructive interference of the signal depending on the frequency, which results in a specific shape of the spectrum for each object position. The simulation model predicts the measurement results for the spectrum in both shape and values. We evaluated our model with the nearest neighbor algorithm, with 97% of the calculated positions within the range of twice the obstacle diameter. Our model predicts the spectrum of a received signal for an ultrasonic transmitter-receiver system in the presence of obstacles. The model is evaluated for both short-range communication and free water localization systems. The number of multipath propagation components (reflectors) is adaptable to the environmental conditions, and the model is prepared for applications with complex multipath propagation scenarios. Doppler effects are not yet part of the proposed model.

In the future, we will improve the model parameters, investigate different metrics, and introduce prior knowledge and appropriate filters to increase the precision of the model for applications such as object localization or wireless underwater communication. We propose our model for buried object localization applications, e.g., cable tracking or detection of unexploded ordnances. Since our model also takes diffraction into account and processes spectral and phase information, we will expect significant improvements for these applications compared to state-of-the-art systems. Therefore, we will extend the model with refraction layers and adapt the model parameters. Furthermore, the model will be applied for object localization applications based on neural networks. Applying the data generated by our model to train neural networks will reduce time and costs.

Acknowledgment

The authors are the members of the Center of Excellence CoSA (Communications-Systems-Applications) at the Department of Electrical Engineering and Computer Science, Technische Hochschule Lübeck.

References

[1] M. Stojanovic and J. Preisig, "Underwater acoustic communication channels: Propagation models and statistical characterization," *IEEE Commun. Mag.*, vol. 47, no. 1, pp. 84–89, Jan. 2009.

[2] P. A. van Walree, "Propagation and scattering effects in underwater acoustic communication channels," *IEEE J. Ocean. Eng.*, vol. 38, no. 4, pp. 614–631, Oct. 2013.

[3] T. Szyrowski, S. K. Sharma, R. Sutton, and G. A. Kennedy, "Developments in subsea power and telecommunication cables detection: Part 1—Visual and hydroacoustic tracking," *Underwater Technol.*, vol. 31, no. 3, pp. 123–132, Jul. 2013.

[4] D. B. Kilfoyle and A. B. Baggeroer, "The state of the art in underwater acoustic telemetry," *IEEE J. Ocean. Eng.*, vol. 25, no. 1, pp. 4–27, Jan. 2000.

[5] N. T. Hossain, R. M. Khan, and S. Rahman, "3-dimensional mapping of underwater surface for navigation using underwater ultrasonic piezoelectric transducer," Ph.D. dissertation, Dept. Elect. Electron. Eng., BRAC Univ., Dhaka, Bangladesh, 2017.

[6] C. Juan and J. Hu, "Single-object localization using multiple ultrasonic sensors and constrained weighted least-squares method," *Asian J. Control*, vol. 23, no. 3, pp. 1171–1184, May 2021.

[7] L. Freitag, M. Johnson, and D. Frye, "High-rate acoustic communications for ocean observatories-performance testing over a 3000 m vertical path," in *Proc. OCEANS MTS/IEEE Conf. Exhib.*, vol. 2, Sep. 2000, pp. 1443–1448.

[8] M. Stojanovic and J. Preisig, "Underwater acoustic communication channels: Propagation models and statistical characterization," *IEEE Commun. Mag.*, vol. 47, no. 1, pp. 84–89, Jan. 2009, doi: 10.1109/MCOM.2009.4752682.

[9] T. C. Yang, "Properties of underwater acoustic communication channels in shallow water," *J. Acoust. Soc. Amer.*, vol. 131, no. 1, pp. 129–145, Jan. 2012.

[10] M. Cimdins, S. O. Schmidt, and H. Hellbrück, "MAMPI-UWB—Multipath-assisted device-free localization with magnitude and phase information with UWB transceivers," *Sensors*, vol. 20, no. 24, p. 7090, 2020.

[11] M. Cimdins and H. Hellbrück, "Modeling received signal strength and multipath propagation effects of moving persons," in *Proc. 14th Workshop Positioning, Navigat. Commun. (WPNC)*, Oct. 2017, pp. 1–6.

[12] F. John, R. Kusche, F. Adam, and H. Hellbrück, "Differential ultrasonic detection of small objects for underwater applications," in *Proc. Global Oceans*. Singapore: US Gulf Coast, 2020, pp. 1–7.

[13] C. Capus, Y. Pailhas, K. Brown, J. Evans, and D. Willins, "Underwater detection classification and tracking using wideband sonar," in *Proc. 3rd Int. Conf. Exhib. Underwater Acoustic Meas., Technol. Results*, 2009, pp. 1–8.

[14] C. Capus, Y. Pailhas, K. Brown, and D. Lane, "Detection of buried and partially buried objects using a bio-inspired wideband sonar," in *Proc. IEEE OCEANS*, May 2010, pp. 1–6.

[15] M. M. Bronstein, A. M. Bronstein, M. Zibulevsky, and H. Azhari, "Reconstruction in diffraction ultrasound tomography using nonuniform FFT," *IEEE Trans. Med. Imag.*, vol. 21, no. 11, pp. 1395–1401, Nov. 2002.

[16] F. Simonetti, L. Huang, N. Duric, and P. Littrup, "Diffraction and coherence in breast ultrasound tomography: A study with a toroidal array," *Med. Phys.*, vol. 36, no. 7, pp. 2955–2965, Jul. 2009.

[17] X. Pan, "Unified reconstruction theory for diffraction tomography, with consideration of noise control," *J. Opt. Soc. Amer. A, Opt. Image Sci.*, vol. 15, no. 9, pp. 2312–2326, 1998.

[18] A. J. Devaney, "Geophysical diffraction tomography," *IEEE Trans. Geosci. Remote Sens.*, vol. GRS-22, no. 1, pp. 3–13, Jan. 1984.

[19] M. Spies, H. Rieder, A. Dillhöfer, V. Schmitz, and W. Müller, "Synthetic aperture focusing and time-of-flight diffraction ultrasonic imaging—Past and present," *J. Nondestruct. Eval.*, vol. 31, no. 4, pp. 310–323, 2012.

[20] F. A. Ravenscroft, K. Newton, and C. B. Scruby, "Diffraction of ultrasound by cracks: Comparison of experiment with theory," *Ultrasonics*, vol. 29, no. 1, pp. 29–37, Jan. 1991.

[21] J. S. von Deimling, P. Held, P. Feldens, and D. Wilken, "Effects of using inclined parametric echosounding on sub-bottom acoustic imaging and advances in buried object detection," *Geo-Mar. Lett.*, vol. 36, no. 2, pp. 113–119, Apr. 2016.
[22] J. Wunderlich, G. Wendt, and S. Müller, "High-resolution echo-sounding and detection of embedded archaeological objects with nonlinear sub-bottom profilers," *Mar. Geophys. Res.*, vol. 26, nos. 2–4, pp. 123–133, Jun. 2005.
[23] J. E. Piper, K. W. Commander, E. I. Thorsos, and K. L. Williams, "Detection of buried targets using a synthetic aperture sonar," *IEEE J. Ocean. Eng.*, vol. 27, no. 3, pp. 495–504, Jul. 2002.
[24] E. Jordan and K. Balmain, *Electromagnetic Waves and Radiating Systems*. Upper Saddle River, NJ, USA: Prentice-Hall, 1968.
[25] M. Cimdins, S. O. Schmidt, and H. Hellbrück, "Modeling the magnitude and phase of multipath UWB signals for the use in passive localization," in *Proc. 16th Workshop Positioning, Navigat. Commun. (WPNC)*, Oct. 2019, pp. 1–6.
[26] R. M. Warner, *Spectral Analysis of Time-Series Data*. New York, NY, USA: Guilford Press, 1998.
[27] (2020). *Hydrophone TC4013—Miniature Reference Hydrophone*. Accessed: Mar. 3, 2021. [Online]. Available: http://www.teledynemarine.com/Lists/Downloads/RESON/Hydrophones/TC4013%20product%20leaflet.pdf
[28] T. Li, H. Wang, Y. Shao, and Q. Niu, "Channel state information–based multi-level fingerprinting for indoor localization with deep learning," *Int. J. Distrib. Sensor Netw.*, vol. 14, no. 10, pp. 1–12, 2018.

Fabian John received the Dipl.-Ing. degree in electrical engineering from Hamburg University of Technology, Germany, in 2012. He is currently pursuing the Ph.D. degree in electrical engineering with Technische Hochschule Lübeck, Germany.

He absolved the certificate program in medical physics and engineering certificate program at the University of Technology in Kaiserslautern, Germany. From 2012 to 2016, he was a Team and the Project Leader of Test Engineering of Electronic Components for Automotive Industries at cbb software GmbH, Lübeck, Germany. From 2016 to 2019, he was a Development Engineer for Production and Quality Assurance Tools for Medical Laboratory Devices at Euroimmun, a PerkinElmer company, Lübeck. Since 2019, he has been a Research Associate with the Center of Excellence CoSA, Technische Hochschule Lübeck, Germany. His research interests include contactless object detection and localization in underwater and medical applications.

Marco Cimdins received the B.Sc. degree in electrical engineering from Technische Hochschule Lübeck, Germany, the B.S.E.E. degree from Milwaukee School of Engineering, Milwaukee, USA, in 2015, and the M.Sc. degree in applied information technology from Technische Hochschule Lübeck in 2017, where he is pursuing the Ph.D. degree.

Since 2017, he has been a Research Associate with the Center of Excellence CoSA. His research interests include device-free localization, indoor localization, and radiofrequency propagation.

Horst Hellbrück received the Diploma degree in electrical engineering from the University of Saarland in 1994 and the Ph.D. degree in computer science from the Technical University of Braunschweig in 2004 in *ad-hoc* networking.

He worked as a Software Engineer at Dräger, Lübeck, from 1994 to 1998, and International Product Marketing at Eupec, Warstein, from 1998 to 2000. He joined the International University in Germany, Bruchsal, in 2000. Before starting his professorship in communication systems and distributed systems at Technische Hochschule Lübeck in 2008, he held a position as a Postdoctoral Researcher at the Institute of Telematics, University of Lübeck. Since December 2013, he has been the Head of the Center of Excellence CoSA. In 2016, he was appointed as an Adjunct Professor at the Institute of Telematics, University of Lübeck. He is a Professor with Technische Hochschule Lübeck, Germany. His research interests are modern structures like wireless mobile networks and sensor networks. His special interests are sensor networks in various application fields, from medical applications to underwater technologies.